2014 American Control Conference (ACC)
June 4-6, 2014. Portland, Oregon, USA

Bounded Droop Controller for Accurate Load Sharing Among Paralleled Inverters

George C. Konstantopoulos, Qing-Chang Zhong, Beibei Ren, and Miroslav Krstic

Abstract— **When paralleled inverters feed a common load, it is required that the load is shared according to their power ratings. In this paper, the robust droop controller (RDC) proposed in the literature for achieving accurate proportional power sharing for paralleled inverters is implemented in a way to ensure a bounded closed-loop performance. Using non-linear Lyapunov methods, it is shown that the controller structure permits the control input to stay within a predefined range. While maintaining the main theory of the RDC, the proposed bounded droop controller (BDC) is proven to guarantee the stability of the closed-loop system in the sense of boundedness for the general load case given in the generalized dissipative Hamiltonian form, which can describe both linear and non-linear load dynamics. Extended simulation results for two single-phase inverters operated in parallel are presented to verify the effectiveness of the BDC for both a linear and a non-linear load case scenario.**

I. INTRODUCTION

The local integration of renewable sources to the electrical network, which is accomplished using suitable power electronic devices (inverters), along with energy storage devices and local loads form a microgrid [1], [2], [3]. In microgrids, due to the limited availability of high current power electronic devices, inverters should be operated in parallel. In order to avoid circulating currents among the converters, droop control methodology [1], [2], [4], [5] is applied, which does not require external communication mechanism among the inverters [6], [7].

One of the main issues in microgrid operation is the accurate power sharing among the paralleled inverters in accordance to their power ratings, which should be maintained in both grid-connected and stand-alone operation. Especially in stand-alone mode, load sharing according to each inverter size under different operating conditions is a challenging task [8], which is usually achieved using droop control techniques. However, conventional droop controllers introduce inherent limitations in accurate real and reactive power sharing as noted in [9]. Additionally, the inverter output impedance plays a key role in accurate load sharing, since inverters equipped with the conventional droop control are required to have the same per-unit output impedance [10]. Therefore, recently, several control designs have been proposed in order to achieve accurate power sharing among the inverters [11], [12], [13], [14], [15]. Among these techniques, the robust droop controller (RDC) proposed in [15] has been proven to achieve accurate load sharing even if numerical computational errors, disturbances, noises, parameter drifts and component mismatches occur.

Although a lot of research has been done in the field of load sharing, the stability properties of the proposed techniques have not been extensively exploited. Most of the stability analysis has been focused on small-signal modelling and linearization methods [12], [13], [16], which are only valid around a specific equilibrium point (local stability). Several conditions of the local exponential stability for frequency droop control are exploited in [17], where however fixed voltage magnitudes and a purely inductive network are considered. Due to the non-linear structure of the droop controller, it becomes obvious that the non-linear stability analysis is essential for investigating the behavior of paralleled inverters. Recently, the $\mathcal{L}_\infty$ stability of the conventional droop control has been proven in [18] where asymptotic stability of lossless microgrids is also achieved. However, the Kron-reduced network approach is considered, which describes the loads in a linear representation, while instantaneous frequency regulation is assumed for the analysis.

To the best of our knowledge, the non-linear closed-loop system stability using a robust droop control technique, which achieves accurate load sharing, independently from the type of the load (linear or non-linear) has not been solved yet. In this paper, two parallel single-phase inverters feeding a local load are considered. The load is given in the generalized dissipative Hamiltonian form, which represents the general case of a power electronic driven dynamic system [19], [20]. For this system, the RDC proposed in [15] can be considered, since it is proven to achieve the most robust performance. Particularly, in the present work, the RDC is implemented in a way to ensure that the control input stays within a predefined range, without changing the main concept of the initial control design. The controller performance is extensively analyzed using non-linear Lyapunov methods and is proven to achieve a bounded performance. Using $\mathcal{L}_\infty$ stability analysis and the small-gain theorem [21], the stability of the non-linear closed-loop system is guaranteed. This represents a significant superiority with respect to the existing techniques since robust accurate load sharing is achieved with a guaranteed stability for the general load

The financial support from the EPSRC, UK under Grant No. EP/J01558X/1 is greatly appreciated.

G. C. Konstantopoulos and Q.-C. Zhong are with the Department of Automatic Control and Systems Engineering, The University of Sheffield, Sheffield, S1 3JD, UK g.konstantopoulos@sheffield.ac.uk, zhongqc@sheffield.ac.uk

B. Ren is with the Department of Mechanical Engineering, Texas Tech University, Lubbock, TX 79409, USA beibei.ren@ttu.edu

M. Krstic is with the Department of Mechanical and Aerospace Engineering, University of California, San Diego, 9500 Gilman Drive, La Jolla, CA 92093-0411, USA krstic@ucsd.edu

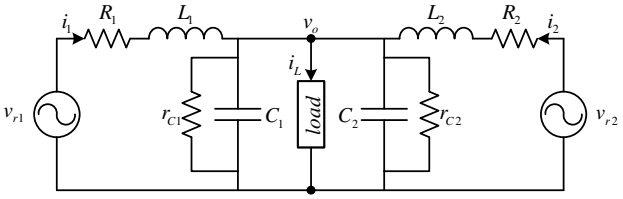

Fig. 1: Schematic diagram of parallel connection of inverters

case. Extensive simulation results for a linear and a non-linear load are illustrated to verify the effectiveness of the proposed BDC compared to the RDC.

The paper is organized as follows. In section II, the dynamic model of the system consisting of two single-phase inverters and a load is obtained along with its properties and the robust droop controller is underlined. In section III, the bounded droop controller is proposed and its performance is investigated. Furthermore, the stability of the closed-loop system is proven using non-linear analysis. In section IV, extensive simulation results are provided to certify the effectiveness of the proposed bounded control scheme while finally, in section V, some conclusions are drawn.

II. Modelling and control of Paralleled inverters

A. Dynamic model

Figure 1 represents the schematic diagram of two single-phase paralleled inverters connected to a common load. An LC filter is assumed at the output of each inverter where L_1, L_2 and C_1, C_2 are the filter inductances and capacitances respectively for each inverter. In practice, each inductor and capacitor introduces parasitic resistances represented as R_1 and R_2 in series with the inductors (typically very small) and r_{C1} and r_{C2} in parallel with the capacitors (typically very large). Variables v_{r1}, v_{r2} and i_1, i_2 are the inverter output voltages and currents respectively while v_o and i_L are the load voltage and current respectively. It should be noticed that the capacitors along with the parasitic resistances can be assumed as a part of the load and therefore, C_1, C_2, r_{C1} and r_{C2} can represent some of the load characteristics as well [9].

The dynamic equations of the system are given as:

$$\begin{aligned} L_1\frac{di_1}{dt} &= -R_1 i_1 - v_o + v_{r1} \\ L_2\frac{di_2}{dt} &= -R_2 i_2 - v_o + v_{r2} \\ (C_1+C_2)\frac{dv_o}{dt} &= i_1 + i_2 - \frac{r_{C1}+r_{C2}}{r_{C1}r_{C2}}v_o - i_L \end{aligned} \tag{1}$$

Since in practice most of the loads are fed by power electronic devices (power converters), then by using average analysis [19], the load can be represented by the generalized dissipative Hamiltonian form [19], [20]:

$$M\dot{w} = \left(J\left(w,\mu(t)\right) - R\right)w + Gv_o \tag{2}$$

where $w = \left[\begin{array}{cccc} i_L & w_1 & w_2 \ldots & w_{m-1}\end{array}\right]^T \in \mathcal{R}^m$ represents the states of the load and $\mu(t)$ is a time-varying bounded vector in a closed set which describes the duty-ratio signals of the converters. Matrix M is constant positive definite, J is skew-symmetric, R is constant and positive definite and $G = \left[\begin{array}{cc} 1 & 0_{1\times(m-1)}\end{array}\right]^T$. For the load equation (2), the load voltage can be considered as an input for the load system (in fact this is usually the case when for example a voltage source device is connected at the inverter's output). It should be also noted that all non-linearities of the load and the bounded duty-ratio signals $\mu(t)$ are restricted into the skew-symmetric matrix J. This is a common issue in power systems, especially for power converter-fed loads [19], [20], [22]. As a result, the complete plant system can be written into the generalized dissipative Hamiltonian form:

$$\tilde{M}\dot{\tilde{x}} = \left(\tilde{J}\left(\tilde{x},\mu(t)\right) - \tilde{R}\right)\tilde{x} + \tilde{G}u \tag{3}$$

where the state vector is $\tilde{x} = \left[\begin{array}{cccc} i_1 & i_2 & v_o & w^T\end{array}\right]^T$, the input vector is $u = \left[\begin{array}{cc} v_{r1} & v_{r2}\end{array}\right]^T$ and matrices $\tilde{M}$, $\tilde{J}$ and $\tilde{R}$ retain the properties already mentioned:

$$\tilde{M} = \begin{bmatrix} L_1 & 0 & 0 & 0_{1\times m} \\ 0 & L_2 & 0 & 0_{1\times m} \\ 0 & 0 & C_1+C_2 & 0_{1\times m} \\ 0_{m\times 1} & 0_{m\times 1} & 0_{m\times 1} & M \end{bmatrix},$$

$$\tilde{J} = \begin{bmatrix} 0 & 0 & -1 & 0 & 0_{1\times(m-1)} \\ 0 & 0 & -1 & 0 & 0_{1\times(m-1)} \\ 1 & 1 & 0 & -1 & 0_{1\times(m-1)} \\ 0 & 0 & 1 & 0 & J_{12}^T \\ 0_{(m-1)\times 1} & 0_{(m-1)\times 1} & 0_{(m-1)\times 1} & -J_{12}^T & J_{22} \end{bmatrix},$$

$$\tilde{R} = \begin{bmatrix} R_1 & 0 & 0 & 0_{1\times m} \\ 0 & R_2 & 0 & 0_{1\times m} \\ 0 & 0 & \frac{r_{C1}+r_{C2}}{r_{C1}r_{C2}} & 0_{1\times m} \\ 0_{m\times 1} & 0_{m\times 1} & 0_{m\times 1} & R \end{bmatrix},$$

$$\tilde{G} = \begin{bmatrix} 1 & 0 & 0_{1\times m} \\ 0 & 1 & 0_{1\times m} \end{bmatrix}^T$$

where $J = \begin{bmatrix} 0 & J_{12} \\ -J_{12}^T & J_{22} \end{bmatrix}$ with J_{12} and J_{22} being $1\times(m-1)$ and $(m-1)\times(m-1)$ matrices respectively.

B. Robust droop controller (RDC)

Droop control is a common power sharing technique for inverters operated in parallel. However, conventional droop control techniques fail to achieve accurate power sharing when the two inverters do not introduce the same per-unit output impedances [9]. This problem can be solved using a robust droop control (RDC) technique as proposed in [15] which, for each inverter $(i \in \{1,2\})$, takes the form:

$$\dot{E}_i = K_e\left(E^* - V_o\right) - n_i Q_i \tag{4}$$

$$\dot{\theta}_i = \omega^* - m_i P_i \tag{5}$$

where E_i and θ_i are the RMS value and the angle of the i-th inverter output voltage, E^* and ω^* are the rated voltage and angular velocity respectively, V_o represents the RMS voltage of the load and P_i, Q_i are the real and reactive power delivered at the load by the i-th inverter. Control parameters K_e, n_i and m_i are suitably determined by the

desired voltage and frequency droop ratio [15]. Thus, the control input (inverter output voltage) is given in the form:

$$v_{ri} = \sqrt{2} E_i \sin(\theta_i) \tag{6}$$

However, the controller structure and dynamics are non-linear, while the RMS load voltage is a non-linear function of v_o, i.e $V_o(v_o)$, and the real and reactive powers are also non-linear functions of v_o and i_i, i.e. $P_i(v_o, i_i)$, $Q_i(v_o, i_i)$. This makes it very difficult to directly investigate the stability analysis of the closed-loop system. Several researchers have recently proved the stability of the inverter-based systems but only the conventional droop controller is used and under the assumption of a linear load [17], [18]. To the best of our knowledge, the stability analysis using the robust droop controller which achieves accurate power sharing for a general type of load has not yet been exploited.

III. Controller Design and Analysis

A. Bounded droop controller (BDC)

In order to facilitate the stability analysis of the inverter-based system using the robust droop controller, the RMS voltage dynamics (4) are implemented in the following form, while keeping the main idea intact:

$$\dot{E}_i = (K_e (E^* - V_o) - n_i Q_i) c E_{qi} \tag{7}$$

$$\dot{E}_{qi} = -(K_e (E^* - V_o) - n_i Q_i) c E_i \tag{8}$$

where c is a positive constant. The inverter output voltage is still given from (6) and the dynamics of the angular velocity from (5), since the dynamics of (5) do not affect the bounded property of the control input due to the $\sin(\theta_i)$ function.

It should be mentioned that one extra state variable is added to represent the dynamics of the RMS voltage, while the initial theory of the robust droop controller is maintained.

It becomes clear from (7)-(8) that the controller structure is represented by a nonlinear double integrator scheme, thus acting as an oscillator. In order to understand this fact, the following Lyapunov function candidate is considered:

$$W_i = E_i^2 + E_{qi}^2 \tag{9}$$

where obviously from (7)-(8) it yields $\dot{W}_i = 0$ and equivalently:

$$W_i = W_{i0} = E_{i0}^2 + E_{qi0}^2, \ \forall t \geq 0 \tag{10}$$

where E_{i0} and E_{qi0} denote the initial conditions of the controller states. Therefore, (9) and (10) imply that E_i and E_{qi} form a circle with center the origin O and radius $V_i = \sqrt{E_{i0}^2 + E_{qi0}^2}$ for any V_o and Q_i (Figure 2) and they exclusively move on its circumference with angular velocity given by the expression:

$$\dot{\phi}_i = (K_e (E^* - V_o) - n_i Q_i) c. \tag{11}$$

Also note that the controller state variables E_i and E_{qi} will be bounded in the set $[-V_i, V_i]$ defined by their initial conditions, independently from the angular velocity (11).

At the desired steady-state equilibrium, it holds true [15]:

$$K_e (E^* - V_o^*) - n_i Q_i^* = 0, \tag{12}$$

where V_o^* and Q_i^* are the steady-state values of V_o and Q_i respectively. This equilibrium corresponds to a desired point (E_i^*, E_{qi}^*) on the circle and simply gives:

$$\dot{\phi}_i^* = 0 \tag{13}$$

which shows that the angular velocity will become zero at the steady-state equilibrium and E_i and E_{qi} will eventually stop.

Since in a typical load sharing application, it is desirable that each inverter starts operating with a zero output voltage, the initial conditions of the controller states can be chosen $E_{i0} = 0$ and $E_{qi0} = V_i > 0$ in order for the states to start from a point on the E_{qi}-axis and move clockwise (Figure 2). Assuming that V_i is suitably chosen in order for the radius of the circle to cover the desired steady-state inverter output voltage $E_i^* \in [-V_i, V_i]$, then the controller states will eventually approach the desired equilibrium. As soon as they approach this point on the circle, the angular velocity will be decreasing giving the opportunity for the controller states to converge to the equilibrium (since at the equilibrium eq. (12) holds true). If the controller states pass the desired equilibrium (depending on the plant dynamics), the angular velocity (11) changes sign, thus making the controller states oscillate around the desired point until they finally converge to it. Controller parameter c can obviously improve the transient response since it affects the angular velocity $\dot{\phi}_i$.

It becomes clear that since E_i and E_{qi} are bounded in the interval $[-V_i, V_i]$, then the inverter output voltage v_{ri}, given by (6), is bounded in the interval $\left[-\sqrt{2}V_i, \sqrt{2}V_i\right]$, thus forming a bounded droop controller (BDC) scheme.

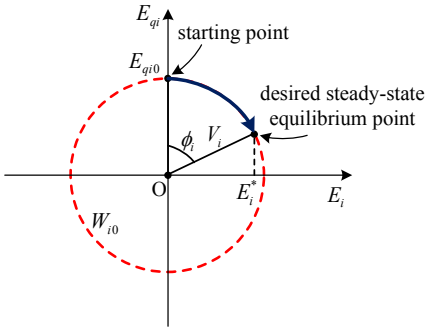

Fig. 2: Controller state performance on $E_i - E_{qi}$ plane

As a result, the closed-loop system becomes:

$$\dot{\bar{x}} = \begin{bmatrix} -\frac{R_1}{L_1} i_1 - \frac{1}{L_1} v_o + \frac{\sqrt{2} E_1 \sin(\theta_1)}{L_1} \\ -\frac{R_2}{L_2} i_2 - \frac{1}{L_2} v_o + \frac{\sqrt{2} E_2 \sin(\theta_2)}{L_2} \\ \frac{1}{C_1+C_2} i_1 + \frac{1}{C_1+C_2} i_2 - \frac{r_{C1}+r_{C2}}{(C_1+C_2) r_{C1} r_{C2}} v_o - \frac{1}{C_1+C_2} i_L \\ M^{-1} G v_o + M^{-1} (J(w, \mu(t)) - R) w \\ (K_e (E^* - V_o(v_o)) - n_1 Q_1(v_o, i_1)) c E_{q1} \\ -(K_e (E^* - V_o(v_o)) - n_1 Q_1(v_o, i_1)) c E_1 \\ (K_e (E^* - V_o(v_o)) - n_2 Q_2(v_o, i_2)) c E_{q2} \\ -(K_e (E^* - V_o(v_o)) - n_2 Q_2(v_o, i_2)) c E_2 \\ \omega^* - m_1 P_1(v_o, i_1) \\ \omega^* - m_2 P_2(v_o, i_2) \end{bmatrix} \tag{14}$$

where $\bar{x} = \left[i_1 \ i_2 \ v_o \ w^T \ E_1 \ E_{q1} \ E_2 \ E_{q2} \ \theta_1 \ \theta_2\right]^T = \left[x_{cl}^T \ \theta_1 \ \theta_2\right]^T$ is the closed-loop state vector.

B. Closed-loop system stability analysis

From the closed-loop system form (14), it becomes obvious that the closed-loop system can be investigated as a feedback interconnection of the plant system and the controller system (Figure 3).

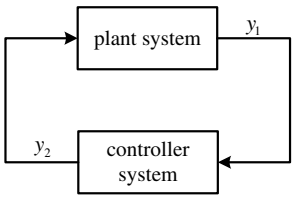

Fig. 3: Closed-loop system in feedback interconnection form

Closed-loop system stability will be investigated in the sense of boundedness and therefore the dynamics of θ_1 and θ_2 can be omitted. This is because $\sin(\theta_i)$ is bounded independent from θ_i and therefore θ_1 and θ_2 can be considered as two time varying signals for the stability analysis. However, the frequency dynamics, although omitted from the stability analysis, are very important for the existence of the equilibrium point as already mentioned in [17].

As a result, the plant system is given in the form:

$$\tilde{M}\dot{\tilde{x}} = \left(\tilde{J}\left(\tilde{x}, \mu(t)\right) - \tilde{R}\right)\tilde{x} + \tilde{G}y_2, \tag{15}$$

$$y_1 = \begin{bmatrix} i_1 & i_2 & v_o \end{bmatrix}^T \tag{16}$$

while the controller system is given in the form:

$$\begin{bmatrix} \dot{E}_1 \\ \dot{E}_{q1} \\ \dot{E}_2 \\ \dot{E}_{q2} \end{bmatrix} = \begin{bmatrix} A_1(y_1) & 0_{2\times 2} \\ 0_{2\times 2} & A_2(y_1) \end{bmatrix} \begin{bmatrix} E_1 \\ E_{q1} \\ E_2 \\ E_{q2} \end{bmatrix}, \tag{17}$$

$$y_2 = \begin{bmatrix} \sqrt{2}E_1 \sin(\theta_1(t)) \\ \sqrt{2}E_2 \sin(\theta_2(t)) \end{bmatrix} \tag{18}$$

with

$$A_1(y_1) = \begin{bmatrix} 0 & \dot{\phi}_1 \\ -\dot{\phi}_1 & 0 \end{bmatrix}, A_2(y_1) = \begin{bmatrix} 0 & \dot{\phi}_2 \\ -\dot{\phi}_2 & 0 \end{bmatrix}.$$

Now, we proceed with the following proposition which shows the stability of the closed-loop system in the sense of boundedness.

Proposition 1: The closed-loop system of Figure 3 with the plant system given by (15)-(16) and the controller system given by (17)-(18), is stable and the closed-loop system solution $x_{cl}(t)$ is bounded for all $t \geq 0$.

Proof: The main task is to prove boundedness of the closed-loop system solution, thus the analysis will be conducted in $\mathcal{L}_\infty$ space. We investigate initially the plant system dynamics given by (15) or equivalently (3) by considering the following Lyapunov function candidate:

$$V(\tilde{x}) = \frac{1}{2}\tilde{x}^T\tilde{M}\tilde{x}. \tag{19}$$

Then the time derivative of V is calculated as:

$$\begin{aligned} \dot{V} &= -\tilde{x}^T\tilde{R}\tilde{x} + \tilde{x}^T\tilde{G}u \\ &= -R_1 i_1^2 - R_2 i_2^2 - \frac{r_{C1}+r_{C2}}{r_{C1}r_{C2}}v_o^2 - w^T R w + \tilde{x}^T\tilde{G}u \\ &\leq -a\|\tilde{x}\|^2 \ \forall \|\tilde{x}\| > \frac{1}{\lambda_{\min}\{R\}}\|u\| \end{aligned} \tag{20}$$

where a is a positive constant and $\lambda_{\min}\{R\}$ is the minimum eigenvalue of R. Since the Lyapunov function V is radially unbounded, then inequality (20) implies that the plant system is input-to-state stable (ISS) [21] providing:

$$\|\tilde{x}(t)\| \leq \beta\left(\|\tilde{x}(0)\|, t\right) + \frac{1}{\lambda_{\min}\{R\}}\sup_{0\leq\tau\leq t}\|u(\tau)\| \tag{21}$$

where β is a class $\mathcal{KL}$ function.

If one considers the unforced plant system $(u = 0)$, then assuming the same Lyapunov function candidate given from (19), the global exponential stability at the origin can be easily derived and it also holds uniformly since the bounded time-varying signal vector $\mu(t)$ does not affect the analysis. By combining (16) and (21), it yields that there exist non-negative constants γ_{plant} and β_{plant} such that

$$\|y_{1\tau}\|_{\mathcal{L}_\infty} \leq \gamma_{plant}\|y_{2\tau}\|_{\mathcal{L}_\infty} + \beta_{plant} \tag{22}$$

for all $y_2 \in \mathcal{L}^2$ and $\tau \in [0, \infty)$ and as a result the plant system is finite-gain $\mathcal{L}_\infty$ stable with gain γ_{plant} [21].

Now, by investigating the controller system (17)-(18), due to the matrix diagonal structure, one can investigate every controller subsystem ($E_1 - E_{q1}$, $E_2 - E_{q2}$) separately where it is considered that $y_1 \in \mathcal{L}^3$.

Let's begin by investigating the system with $E_1 - E_{q1}$. Considering the Lyapunov function candidate given by (9) and following the analysis described in subsection III-A, it yields that E_i and E_{qi} are bounded in the set $[-V_i, V_i]$ for every bounded input y_1, i.e. there exists non-negative constant β_1 such that

$$\left\| \begin{matrix} E_{1\tau} \\ E_{q1\tau} \end{matrix} \right\|_{\mathcal{L}_\infty} \leq \beta_1 \tag{23}$$

Since the bound of the states depends only from the initial condition E_{qi0} and not from the bound of the input y_1, inequality (23) can be written in the form of (22) with zero gain. Therefore, the special structure of the controller proves that the system with $E_1 - E_{q1}$ is finite-gain $\mathcal{L}_\infty$ stable with zero gain.

A similar analysis can prove that the controller subsystem $E_2 - E_{q2}$ is also finite-gain $\mathcal{L}_\infty$ stable with zero gain. As a result, there exists a non-negative constant $\beta_{control}$ such that:

$$\begin{aligned} \|y_{2\tau}\|_{\mathcal{L}_\infty} &= \left\| \begin{matrix} \sqrt{2}E_{1\tau}\sin(\theta_1(t)) \\ \sqrt{2}E_{2\tau}\sin(\theta_2(t)) \end{matrix} \right\|_{\mathcal{L}_\infty} \leq \sqrt{2}\left\| \begin{matrix} E_{1\tau} \\ E_{2\tau} \end{matrix} \right\|_{\mathcal{L}_\infty} \\ &\leq \beta_{control} \end{aligned} \tag{24}$$

which proves that the controller system (17)-(18) is also finite-gain $\mathcal{L}_\infty$ stable with gain $\gamma_{control} = 0$. Then according to the small-gain theorem [21], it holds true that $\gamma_{plant}\gamma_{control} < 1$ and as a result, since no other external

inputs are applied on the system (Figure 3), the closed-loop system solution is bounded. ■

It should be noted that in many load sharing applications, the measuring and processing of the real and reactive powers P_i and Q_i are obtained through low-pass filters [16]. Therefore, it is important to investigate whether the existence of these filters affects the closed-loop system stability analysis. This is discussed in the following remark.

Remark 1: Low-pass filters are always finite-gain $\mathcal{L}_\infty$ stable systems with a finite gain γ_{filter} and they can be represented as a series connection of the controller system in the feedback loop in Figure 3. Since the series connection of two $\mathcal{L}_\infty$ stable systems is also $\mathcal{L}_\infty$ stable with finite gain $\gamma_{filter}\gamma_{control}$ and the controller has zero gain, then obviously the stability analysis is not affected by the filters used.

IV. Simulation results

In order to verify the BDC operation, two single-phase inverters operated in parallel are considered. Each inverter is powered by a $400V$ DC voltage source and the power ratings are $S_1 = 0.5kVA$ and $S_2 = 1kVA$ for inverters 1 and 2 respectively. It is expected that $P_2 = 2P_1$ and $Q_2 = 2Q_1$. Both inverters operate in a switching frequency of $15kHz$ and the line frequency of the system is $50Hz$. The rated voltage of the inverters is $E^* = 230V$ and $K_e = 10$. The filter inductor is $L_1 = L_2 = 2.2mH$ with a parasitic resistance $R_1 = R_2 = 0.3\Omega$ and the filter capacitor $C_1 = C_2 = 10\mu F$ with parasitic resistance $r_{C1} = r_{C2} = 100M\Omega$. According to [23], the desired voltage drop ratio is chosen $\frac{n_i S_i^*}{K_e E^*} = 0.25\%$ and the frequency drop ratio is chosen $\frac{m_i S_i^*}{\omega^*} = 0.1\%$. Therefore, the droop coefficients are calculated as $n_1 = 0.0115$, $n_2 = 0.0057$, $m_1 = 6.2832 \cdot 10^{-4}$ and $m_2 = 3.1416 \cdot 10^{-4}$. Assuming a technical requirement that permits the inverter voltage not to exceed the rated voltage by more than 20% at any time, parameter V_i is chosen equal to $1.2E^* = 276V$, while c is chosen as $c = 0.01$.

Two different scenarios are illustrated with respect to the load structure. In the first case, the load is a 57Ω resistor (linear load), while in the second case a diode rectifier (non-linear load) is considered, loaded by a capacitor $C_L = 800\mu F$ and a resistor $R_L = 100\Omega$. In the ac side, a boosting inductor is used with $L_L = 2.2mH$ and a parasitic resistance $r_L = 0.3\Omega$. The load can be a controllable rectifier as noted in [22], where it is clear that the dynamic load equations satisfy (2). In this work, for simplicity, a diode rectifier is considered which represents a non-linear load as shown in Figure 4. In each scenario, the RDC, as proposed in [15], is compared with the BDC analyzed in the present work.

Figure 5 illustrates the time response of the paralleled inverters system with a linear load for the RDC and the BDC case. Comparing Figure 5a with Figure 5b and Figure 5c with Figure 5d, it is clear that both controllers achieve precise sharing of the real and the reactive power respectively, proportional to the inverters ratings. This underlines their advantage with respect to the conventional droop control techniques. As it can be observed in Figures 5a-5d, the BDC achieves faster regulation at the desired steady-state values due to the controller parameter c. At steady-state values, the BDC performance coincides with the RDC as it can be verified from Figure 5e, thus verifying the fact that the proposed method keeps the RDC theory intact. Figure 5f shows the response of the controller states E_1 and E_{q1} on $E_1 - E_{q1}$ plane where it is clear that they travel on the circle with center the origin and radius equal to $V_1 = 276V$ until they finally converge to the desired steady-state values corresponding to a specific point on the circle. This verifies the controller operation as described in subsection III-A and consequently the stability analysis presented in subsection III-B.

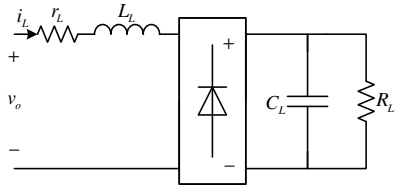

Fig. 4: Non-linear load

Simulation results for the case of the non-linear load are presented in Figure 6. Both the RDC and the BDC share the power accurately while the BDC produces again a bounded performance according to the theoretical investigation for the non-linear load case as well.

V. Conclusions

In this paper, a bounded droop controller was proposed in order to achieve accurate load sharing in paralleled inverters. While maintaining the theory of the RDC, the BDC also introduces a bounded characteristic for the control input which is proven to stay within a predefined range. An extended analysis was presented to certify that the proposed bounded control scheme guarantees the stability of the closed-loop system independently from the type of the load (linear or non-linear). Extended simulation results suitably verified the proposed BDC design approach compared to the RDC.

References

[1] J. Guerrero, Mukul Chandorkar, T. Lee, and P. Loh. Advanced Control Architectures for Intelligent MicroGrids-Part I: Decentralized and Hierarchical Control. *IEEE Trans. Ind. Electron.*, 60(4):1254–1262, Apr. 2013.

[2] J. Guerrero, P. Loh, T. Lee, and Mukul Chandorkar. Advanced Control Architectures for Intelligent Microgrids-Part II: Power Quality, Energy Storage, and AC/DC Microgrids. *IEEE Trans. Ind. Electron.*, 60(4):1263–1270, Apr. 2013.

[3] G. Weiss, Q.-C. Zhong, T. Green, and J. Liang. H^∞ repetitive control of DC-AC converters in micro-grids. *IEEE Trans. Power Electron.*, 19(1):219–230, Jan. 2004.

[4] E. Barklund, N. Pogaku, M. Prodanovic, C. Hernandez-Aramburo, and T.C. Green. Energy management in autonomous microgrid using stability-constrained droop control of inverters. *IEEE Trans. Power Electron.*, 23(5):2346–2352, Sept. 2008.

[5] J. M. Guerrero, J. C. Vasquez, J. matas, L. Garcia de Vicuna, and M. Castilla. Hierarchical control of droop-controlled AC and DC microgrids- a general approach towards standardization. *IEEE Trans. Ind. Electron.*, 58(1):158–172, Jan. 2011.

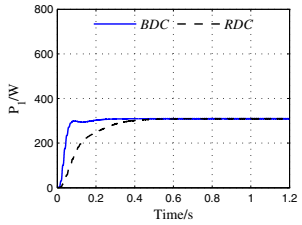

(a) real power of inv. 1

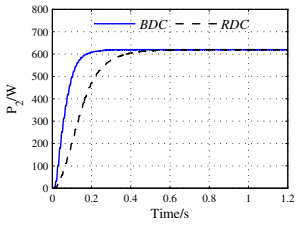

(b) real power of inv. 2

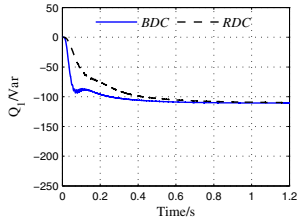

(c) reactive power of inv. 1

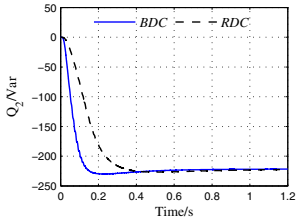

(d) reactive power of inv. 2

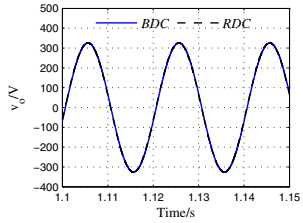

(e) output voltage

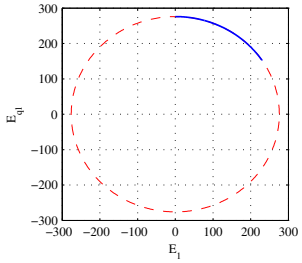

(f) $E_1 - E_{q1}$ plane

Fig. 5: Simulation results with linear load for the RDC and the BDC

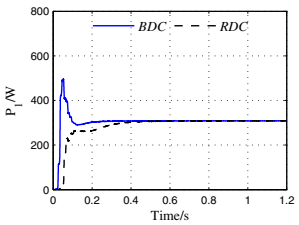

(a) real power of inv. 1

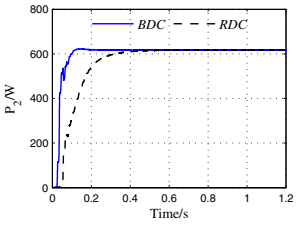

(b) real power of inv. 2

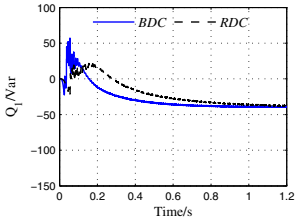

(c) reactive power of inv. 1

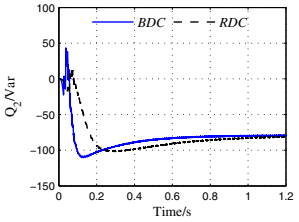

(d) reactive power of inv. 2

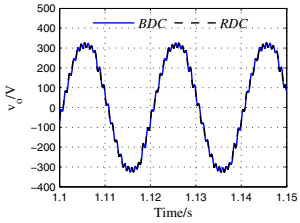

(e) output voltage

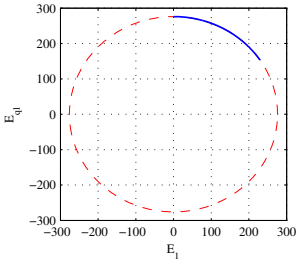

(f) $E_1 - E_{q1}$ plane

Fig. 6: Simulation results with non-linear load for the RDC and the BDC

[6] A. Tuladhar, H. Jin, T. Unger, and K. Mauch. Parallel operation of single phase inverter modules with no control interconnections. In *Proc. of the 12th IEEE Applied Power Electronics Conference and Exposition*, pages 94–100, 1997.

[7] M.C. Chandorkar, D.M. Divan, and R. Adapa. Control of parallel connected inverters in standalone AC supply systems. *IEEE Trans. Ind. Appl.*, 29(1):136–143, Jan./Feb. 1993.

[8] C.K. Sao and P.W. Lehn. Autonomous load sharing of voltage source converters. *IEEE Trans. Power Del.*, 20(2):1009–1016, Apr. 2005.

[9] Q.-C. Zhong and T. Hornik. *Control of Power Inverters in Renewable Energy and Smart Grid Integration*. Wiley-IEEE Press, 2013.

[10] J. M. Guerrero, L. G. de Vicuna, J. Matas, M. Castilla, and J. Miret. Output impedance design of parallel-connected UPS inverters with wireless load-sharing control. *IEEE Trans. Ind. Electron.*, 52(4):1126–1135, May. 2005.

[11] J. M. Guerrero, J. Matas, L. G. de Vicuna, M. Castilla, and J. Miret. Decentralized control for parallel operation of distributed generation inverters using resistive output impedance. *IEEE Trans. Ind. Electron.*, 54(2):994–1004, Nov. 2007.

[12] Y. Mohamed and E.F. El-Saadany. Adaptive decentralized droop controller to preserve power sharing stability of paralleled inverters in distributed generation microgrids. *IEEE Trans. Power Electron.*, 23(6):2806–2816, Nov. 2008.

[13] R. Majumder, B. Chaudhuri, A. Ghosh, G. Ledwich, and F. Zare. Improvement of stability and load sharing in an autonomous microgrid using supplementary droop control loop. *IEEE Trans. Power Syst.*, 25(2):796–808, May 2010.

[14] Y.W. Li and C.-N. Kao. An accurate power control strategy for power-electronics-interfaced distributed generation units operating in a low-voltage multibus microgrid. *IEEE Trans. Power Electron.*, 24(12):2977–2988, Dec. 2009.

[15] Q.-C. Zhong. Robust droop controller for accurate proportional load sharing among inverters operated in parallel. *IEEE Trans. Ind. Electron.*, 60(4):1281–1290, Apr. 2013.

[16] E.A.A. Coelho, P.C. Cortizo, and P.F.D. Garcia. Small-signal stability for parallel-connected inverters in stand-alone AC supply systems. *IEEE Trans. Ind. Appl.*, 38(2):533–542, Oct. 2002.

[17] J. W. Simpson-Porco, F. Dörfler, and F. Bullo. Synchronization and power sharing for droop-controlled inverters in islanded microgrids. *Automatica*, 49(9):2603 – 2611, 2013.

[18] J. Schiffer, R. Ortega, A. Astolfi, J. Raisch, and T. Sezi. Conditions for Stability of Droop-Controlled Inverter-Based Microgrids. *Submitted to Automatica*, 2013.

[19] R. Ortega, Antonio Loria, Per Johan Nicklasson, and Hebertt Sira-Ramirez. *Passivity-based Control of Euler-Lagrange Systems, Mechanical, Electrical and Electromechanical Applications*. Springer-Verlag. Great Britain, 1998.

[20] G. C. Konstantopoulos and A. T. Alexandridis. Generalized Nonlinear Stabilizing Controllers for Hamiltonian-Passive Systems With Switching Devices. *IEEE Trans. Control Syst. Technol.*, 21(4):1479–1488, 2013.

[21] Hassan K. Khalil. *Nonlinear Systems*. Prentice Hall, 2001.

[22] D. Karagiannis, E. Mendes, A. Astolfi, and R. Ortega. An experimental comparison of several PWM controllers for a single-phase AC-DC converter. *IEEE Trans. Control Syst. Technol.*, 11(6):940–947, 2003.

[23] The grid code. Technical report, National Grid Electricity Transmission PLC, Dec. 2010.